Langmuir

Article

pubs.acs.org/Langmuir

JKR Theory for the Stick–Slip Peeling and Adhesion Hysteresis of Gecko Mimetic Patterned Surfaces with a Smooth Glass Surface

Saurabh Das, Sathya Chary,[‡] Jing Yu,[†] John Tamelier,[‡] Kimberly L. Turner,[‡,*] and Jacob N. Israelachvili[†,*]

[†]Department of Chemical Engineering and [‡]Department of Mechanical Engineering, University of California, Santa Barbara, California 93106, United States

Supporting Information

ABSTRACT: Geckos are highly efficient climbers and can run over any kind of surface with impeccable dexterity due to the typical design of their hierarchical foot structure. We have fabricated tilted, i.e., asymmetric, poly(dimethylsiloxane) (PDMS) microflaps of two different densities that mimic the function of the micrometer sized setae on the gecko foot pad. The adhesive properties of these microflaps were investigated in a modified surface forces apparatus; both for normal pure loading and unloading (detachment), as well as unloading after the surfaces were sheared, both along and against the tilt direction. The tilted microflaps showed directional, i.e., anisotropic adhesive behavior when sheared against an optically smooth (RMS roughness ≈ 10 ± 8 nm) SiO_2 surface. Enhanced adhesion was measured after shearing the flaps along the tilted (gripping) direction and low adhesion when sheared against the tilted (releasing) direction. A Johnson–Kendall–Roberts (JKR) theory using an effective surface energy and modulus of rigidity (stiffness) quantitatively described the contact mechanics of the tilted microflaps against the SiO_2 surface. We also find an increasing adhesion and stick–slip of the surfaces during detachment which we explain qualitatively in terms of the density of flaps, considering it to increase from 0% (no flaps, smooth surface) to 100% (close-packed flaps, effectively smooth surface). Large energy dissipation at the PDMS–silica interface caused by the viscoelastic behavior of the polymer results in stick–slip peeling and hence an enhanced adhesion energy is observed during the separation of the microflaps surface from the smooth SiO_2 surface after shearing of the surfaces. For structured multiple contact surfaces, hysteresis as manifested by different loading and unloading paths can be due entirely to the *elastic* JKR micro-contacts. These results have important implications in the design of biomimetic adhesives.

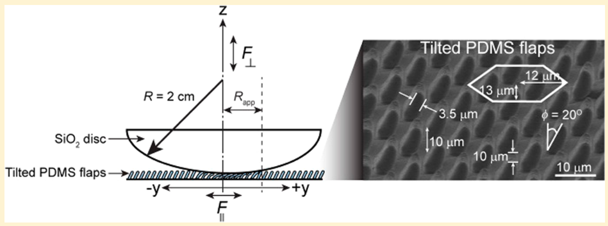

■ INTRODUCTION

The supreme ability of geckos to attach and detach quickly to any surface has been fascinating man for over two millennia. They can attach and detach their toes in matters of millisecond[1] on surfaces, be they vertical or inverted. This exceptional feature of quick attachment and equally quick detachment to any surface is attributed to the typical hierarchical structure of their foot-pad[2] and is still a challenge that no conventional adhesive is capable of meeting. A considerable number of studies have been performed to understand the mechanism of the gecko adhesive system[3−8] and mimic the same for functional surfaces and articulated robotic devices.[9−12]

It has been shown that the geckos employ the universal van der Waals force of adhesion[6,13] and possibly capillary forces[14−18] to attach to surfaces and a peeling mechanism for quick detachment.[4] It has been demonstrated that the hierarchical structure of the gecko foot hair not only allows it to conform to micro and nano scale asperities maintaining high adhesion force on surfaces, but also has anisotropic/directional frictional-adhesion properties.[13,19,20] Various types of patterned hierarchical structures mimicking the gecko foot pad have been fabricated for enhanced adhesion to smooth and rough surfaces.[10,11,21−30] Previous works have shown that tilted micro structures perform most closely to the gecko adhesive system.[11,12,21,22,31,32] However, little effort has been made to understand the effect of the geometry and the areal density of the flaps at the micro level, which is crucial in determining the contact mechanics of the arrays of the flaps to a surface.

Here, we report the mechanism of adhesion of the tilted poly(dimethylsiloxane) PDMS micro flaps to a smooth silica surface with and without prior shearing of the surfaces. Shearing significantly changes the effective adhesion energy (twice that of the theoretical value) of the flaps to the silica surface, and its magnitude is dependent on the sliding direction. The unloading of the (asymmetric and structured) flaps from the silica surface with multiple micro contacts is well described by the classic Johnson–Kendall–Roberts (JKR) theory, unlike the peeling of two smooth PDMS surfaces and, the observed hysteresis and stick–slip has a different origin to that seen between two smooth (unstructured) single contact geo-

Received: September 7, 2013
Revised: October 30, 2013

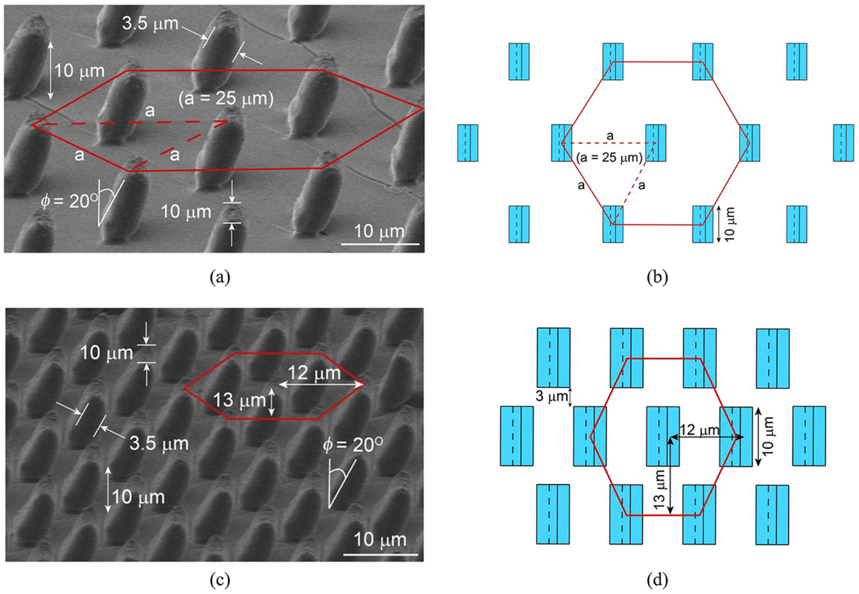

Figure 1. SEM images of the (a) low areal density (1850 flaps/mm^2), 1X tilted PDMS flaps and (c) high areal density (6410 flaps/mm^2), 3.5X tilted PDMS flaps. The flaps are tilted at an angle of 20° from the vertical. Schematic top-view orthographic diagrams showing the positions of the flaps relative to each other for both the (b) 1X flaps and (d) 3.5X flaps.

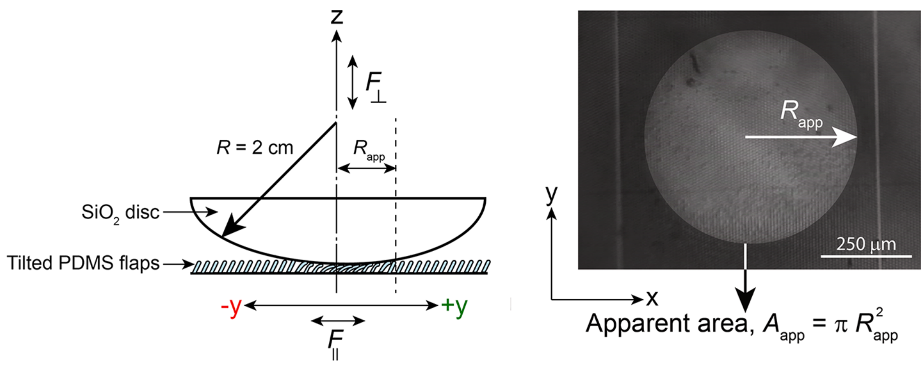

Figure 2. The apparent area, A_{app}, of contact when the arrays of PDMS microflaps are compressed against a spherical silica disc of radius of curvature, R = 2 cm. The bright circular area* shows the region of flaps that is in the deformed state. *Contrast has been enhanced for clarity.

metries.[33] We demonstrate that the effective stiffness of the arrays of the flaps play minor role in determining the adhesion energy. Stick–slip peeling instabilities during separation after prior sliding of the flaps along the direction of the tilt could rationalize the measured high adhesion energies of the PDMS flaps on the silica surface.

■ MATERIALS AND METHODS

Fabricated Patterned Surfaces. Large arrays of tilted PDMS flaps of two different densities (Figure 1), were fabricated using micro fabrication techniques described elsewhere.[10] The low (1X) and the high (3.5X) areal density flaps have 1850 flaps/mm^2 and 6410 flaps/mm^2, respectively. The flaps are tilted at an angle of ϕ = 20° from the vertical. Schematic top-view orthographic diagrams show that the flaps are arranged in a hexagonal packing geometry (Figure 1b,d).

Normal and Lateral Force Measurements. A modified surface forces apparatus (SFA)[34] was used to measure the normal $F_\perp$ (adhesion and loads) and the lateral forces $F_\parallel$ between the arrays of the fabricated microflaps and a spherical silica disc of radius of curvature, R = 2 cm, and RMS roughness ~10 ± 8 nm. The full details of the force measurements have been described in previous work.[10,11] As a summary, the spherical glass disc was mounted to the top friction device, which can slide laterally over a distance of 100—500 μm at different sliding speeds (1—10 μm/s). The PDMS flaps were glued to a flat glass disc, which sits on a double cantilever spring with strain gauges that can measure the normal forces. A CCD camera was mounted on a microscope to visualize the contact area during loading, unloading, and sliding of the spherical silica disc against the arrays of the fabricated PDMS microflaps (Figure 2).

In the SFA experiment, the top spherical silica disc was pressed against the PDMS microflaps at a constant speed of ~10 μm/s until the desired preload, $F_\perp^P$ was reached. Adhesion tests were performed by separating the two surfaces, without them being sheared against each other (no prior shearing). Adhesion was also measured after the surfaces were sheared against each other at a velocity of 10 μm/s along the +y direction (along the direction of the tilt) and −y direction (against the direction of the tilt). Shearing was stopped after sliding for ~300 μm while the surfaces were still under a shear stress (Figure 3). The flaps did not get damaged even after many sliding cycles (50−100) at a given contact point and the adhesion tests were reproducible at different contact points. Measurements and surface preparations were performed in a clean dust free environment (sealed SFA or in Laminar flow hood).

Theoretical Background. A brief description of the contact mechanics between two bodies in adhesive contact will be helpful in interpreting the experimental data, since this work investigates the effect of shear on the change in the adhesion properties of a patterned surface against a smooth silica disc.

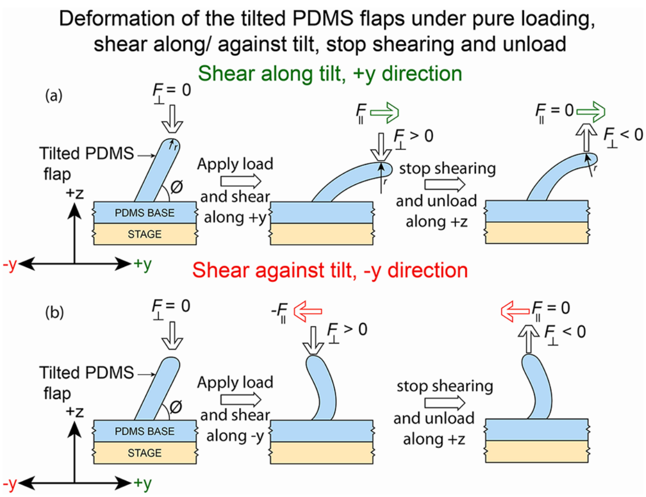

Figure 3. Schematics of a single flap deformation showing the separation of the flap with the upper silica surface after the flaps are sheared (a) along the direction of the tilt (+y direction) (b) against the direction of the tilt (−y direction). The adhesion forces, $-F_\perp$ measured after sliding the top surface in the +y direction are significantly higher than the values measured after sliding in the −y direction.

Classical mechanics deals solely with bulk materials, whereas contact mechanics takes into account the bulk properties along with the surface and geometry of contact. Geometric effects of local elastic deformation were first considered by Hertz,[35] and the effect of adhesive interactions were neglected. An improvement over the Hertzian theory is the Johnson−Kendall−Roberts (JKR) theory,[36] in which the contact surfaces are considered to be adhesive. The adhesion force (F_{ad}) between a sphere of radius r and a plane in the JKR model is given by the following:

$$F_{ad} = \frac{3}{2}\pi r W_{12} \tag{1}$$

where $W_{12} = \gamma_1 + \gamma_2 - \gamma_{12}$ is the thermodynamic work of adhesion, and γ_1, γ_2, and γ_{12} are the surface and interfacial energies of two interacting surfaces.

A JKR experiment involves bringing two surfaces (a sphere and a plane) into contact by applying an external load followed by retraction until the contact is broken. The deformation of the surfaces at a specified load $F_\perp$ is described by the contact area of radius a as a result of compression (and adhesion). The expression for a is given by the following:[36]

$$a = \pi\left\{\frac{r}{K_{eff}}\left[F_\perp + 6\pi r W_{12} + \left(12\pi r W_{12} F_\perp + (6\pi r W_{12})^2\right)^{1/2}\right]\right\}^{2/3} \tag{2}$$

$$\frac{1}{K_{eff}} = \frac{3}{4}\left(\frac{1-\nu_1^2}{E_1} + \frac{1-\nu_2^2}{E_2}\right) \tag{3}$$

where K_{eff} is the effective stiffness, ν_i and E_i are the Young's modulus and the Poisson's ratio of the samples 1 and 2, respectively.

RESULTS AND DISCUSSION

Adhesion Force Measurement with No Prior Shearing. The adhesion behavior of the low (1X) and the high (3.5X) areal density PDMS microflaps were tested against a smooth spherical silica disc at different preloads of $F_\perp^P = 1 - 40$ mN. The 1X flaps showed no measurable adhesion ($F_{ad} < 0.1$ mN) to the silica surface which is consistent with our previous work (Figure 4).[11] The graph of apparent area, A_{app} vs the normal actual load, $F_\perp^P$ for the 1X flaps showed no hysteresis between the loading and unloading curves (Figure 4), which is a characteristic signature of nonadhesive contact. This observation is attributed to the high surface roughness (RMS roughness ≈ 250 nm) of the top edge of the 1X flaps (as visualized in the SEM) that reduces the real area of contact between the flaps and the spherical silica surface. The effective stiffness, K_{eff} of the 1X (low density) PDMS microflaps was calculated to be 1 MPa by JKR sphere on flat geometry fit (eqs 1−3) to the experimental data (Figure 4). The calculated value for K_{eff} is significantly higher than the expected value for bulk PDMS (∼300 kPa) and is attributed to the nonlinear strain response to the applied stress for the PDMS material (see Supporting Information, SI, Figure S1).

The 3.5X (high density) PDMS microflaps showed an adhesion force of $F_{ad} = 0.8$ mN against the silica disc (Figure 5). SEM images show that these flaps have lower surface roughness for the top edge of the flaps (RMS roughness ∼170 nm). The

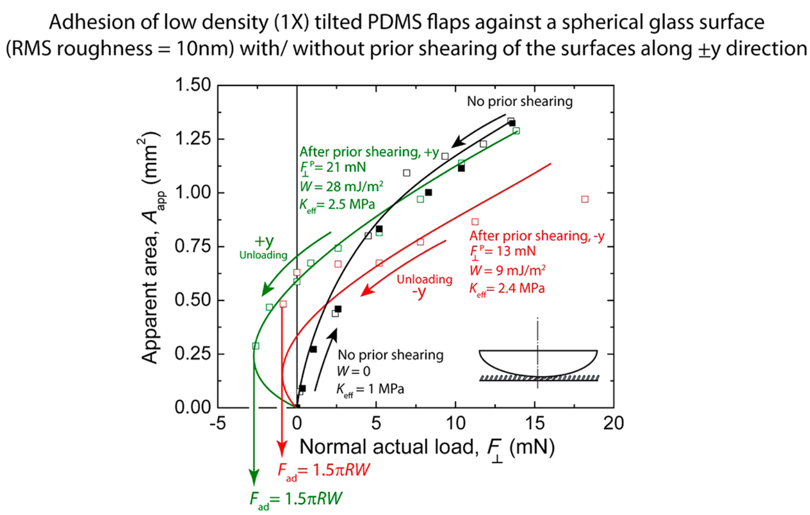

Figure 4. The apparent area, A_{app} vs the normal actual load, $F_\perp$ for the 1X tilted PDMS microflaps as they are separated (unloaded) from the spherical silica surface of radius of curvature, $R = 2$ cm. The open squares represent the experimentally observed A_{app} when unloading the flaps from the silica surface. The curves show the JKR fits to the experimental data.

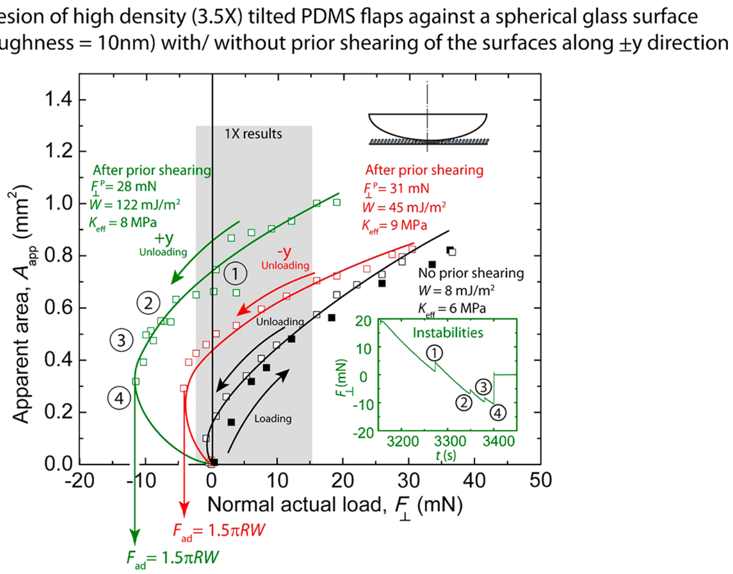

Figure 5. The apparent area, A_{app} vs the normal actual load, $F_\perp$ for the 3.5X tilted PDMS microflaps as they are separated (unloaded) from the spherical silica surfaceof radius of curvature, R = 2 cm. The open squares represent the experimentally observed A_{app} when unloading the flaps from the silica surface. The curves show the JKR fits to the experimental data. As a comparison, the area of the plot occupied by the curves for the 1X tilted PDMS microflaps is also shown by the shaded gray box.

lower surface roughness and the high areal density result in better commensurability between the surfaces and hence superior adhesion of the 3.5 X PDMS microflaps against the silica surface. The plot of A_{app} vs $F_\perp^P$ for the 3.5X flaps was hysteretic with K_{eff} = 6 MPa and an effective value for the work of adhesion of W = 8 mJ/m^2. This effective work of adhesion is an outcome of the decreasing energy due to the formation of bonds between the surfaces at the expense of the elastic deformation energy which reduces the binding energy.

The adhesion force per flap, f_{ad}, was calculated to be 1 μN with a real area of contact per flap of a_{real} = 5 μm^2, and the local radius of curvature at pull-off was r = 5 μm (Table 1) for the

Table 1. Sphere on Flat JKR Model for Individual Flap Deformation

	1X tilted PDMS flaps (±15%)			3.5X tilted PDMS flaps (±15%)		
per flap JKR parameters	no shear	+y shear	−y shear	no shear	+y shear	−y shear
calculated number of flaps at pull off, n^a	–	**530**	830	640	**2040**	1870
calculated adhesion force, f_{ad} (μN)^b	–	**5**	1	1	**6**	2
JKR radius of curvature, r (μm)^c	–	20	4	5	23	9
calculated real area of contact, a_{real} (μm^2)^d	–	**31**	4	5	**37**	11

[a]Calculated from the measured apparent area of contact, A_{app} using the equation, $n = A_{app}/\sigma$ where σ = Flap density (1850 flaps/mm^2 for 1X tilted PDMS flaps and 6410 flaps/mm^2 for 3.5X tilted PDMS flaps) [b]Calculated from the measured force at pull off (total adhesion force), F_{ad} using the equation, $f_{ad} = F_{ad}/n$ [c]Calculated from the JKR sphere on a flat model using eq 1). [d]Calculated from the JKR sphere on a flat model using equation (2, where, $1/K = 3/4(k_{PDMS} + k_{glass})$. Now, $k_{PDMS} = ((1-\nu_{PDMS}^2)/E_{PDMS})$; $k_{glass} = (1-\nu_{glass}^2/E_{glass})$, since E_{PDMS}(1.8 MPa) ≪ E_{glass}(50 GPa). Hence, $1/K \approx 3/4\ k_{PDMS} = 3/4((1-\nu_{PDMS}^2)/E_{PDMS}) = 3/4\ (1-0.5^2)/1.8)$. → K = 3.2 MPa. Therefore, the fitted stiffness, K to the JKR sphere on flat model in eq 2 for the individual flaps is 3.2 MPa.

3.5X flaps during pure loading and unloading (no shear). The Hamaker constant for PDMS and silica interacting across dry air is 5.3 × 10^{-20} J.[37] Hence, the adhesive pressure, P_{ad} between PDMS and silica is, $P_{ad} = (A/6\pi D^3) = 6.3 \times 10^8$ N/m^2, where D = 0.165 nm is the intermolecular distance. Thus, the theoretically calculated force of interaction between one flap and the silica surface due to van der Waals force is $f_{ad}^{theory} = a_{real}P_{ad}$ = 3 mN. This is about 3 orders of magnitude bigger than the experimentally observed value for f_{ad} and shows how roughness can significantly decrease the adhesive force of interaction between two surfaces.[10,38,39]

The measured pull off force depends on the modulus of rigidity of the surfaces as well as the surface roughness,[40] and the length scale, $\lambda = W/K_{eff}$ determines the range over which the attractive adhesive force dominates the repulsive elastic force.[41,42] The higher the value for λ, the more compliant the surfaces are and the stronger the adhesive force of interaction is between the surfaces. The effective stiffness of the 3.5X (high density) PDMS microflaps is ~3.5 times larger than that of the 1X (low density) microflaps; however, the former flaps showed adhesion to the silica surface and the latter one does not. This is because λ for the 1X and the 3.5X PDMS microflaps are ~0 and 1.3 nm respectively, i.e., the elastic strain energy between the 1X PDMS microflaps and the silica surface always dominates over the adhesive energy if the surfaces are separated without prior sliding.

Adhesion Force Measurement with Prior Shearing. Shearing the arrays of the tilted PDMS microflaps against the silica sphere significantly increased the adhesive force of interaction between the two surfaces. For the 1X (low density) microflaps, effective adhesion energies of W = 28 mJ/m^2 and 9 mJ/m^2 were obtained for prior shearing of the flaps against the silica surface along the +y (along the tilted direction or gripping direction) and the −y directions (against the tilted direction or releasing direction), respectively (Figure 4). The high density 3.5X microflaps exhibited much larger W of 122 mJ/m^2 and 45 mJ/m^2, respectively, for prior shearing the flaps against the silica surface along the +y and −y directions (Figure 5). The experimentally observed W for the 3.5X microflaps is higher than that expected between a smooth PDMS and silica surface calculated by van der Waals theory (W = 50 mJ/m^2).[37] This can be attributed to the bond formation due to local molecular adhesion between the siloxane groups of the PDMS with the silica surface and has been previously observed in rubber sliding on hard surfaces.[43]

Slip instabilities were observed at the PDMS flaps-silica interface during unloading after prior shearing along the +y direction (along the direction of the tilt) for both the flap densities (Figure 6). The magnitudes of these instabilities were

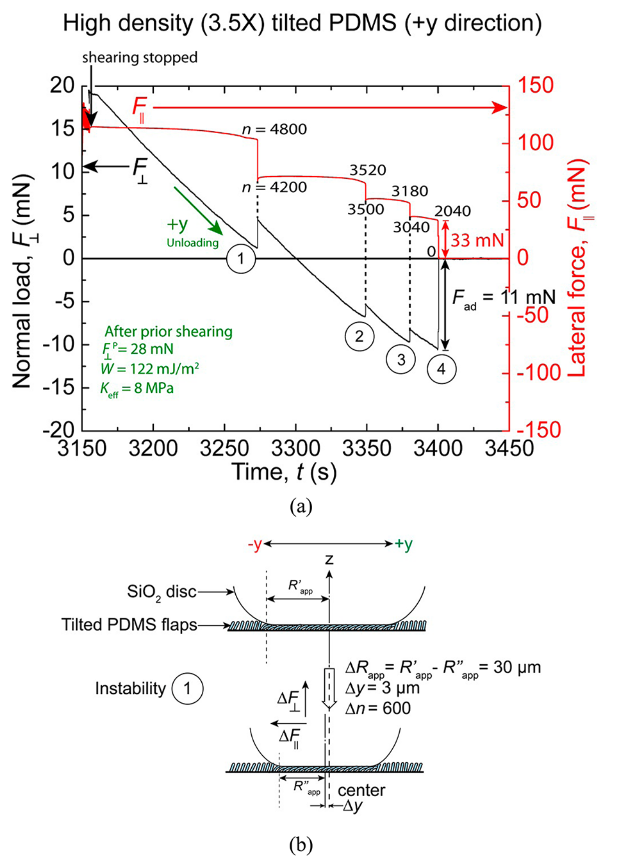

Figure 6. (a) Real time normal load and lateral force (friction) measurement of the high density (3.5X) tilted PDMS flaps against a spherical glass surface (RMS roughness = 1 nm) with prior shearing of the surfaces along the +y direction. Here, n gives the number of the tilted microflaps in contact with the glass surface just before and after the instability jumps. (b) Schematics of the contact just before and after the instability jump at 1.

bigger for the 3.5X (high density) microflaps relative to the 1X (low density) microflaps (see SI Figure S2). This can be attributed to the larger number of flaps detaching from the PDMS−SiO_2 interface for the 3.5X microflaps compared to the 1X microflaps during the separation of the two surfaces, as illustrated in Figure 7. Theoretically, the stick−slip instability should reach a maximum value on increasing the flaps coverage, then decrease and eventually disappear for 100% coverage (close-packed flaps) which can be considered to be an effectively smooth surface, as in the case of zero coverage (Figure 7). No slip instabilities were recorded for unloading after prior shearing along the −y direction (against the direction of the tilt). Hence, another possible explanation for the high observed value of W for the 3.5X microflaps after prior

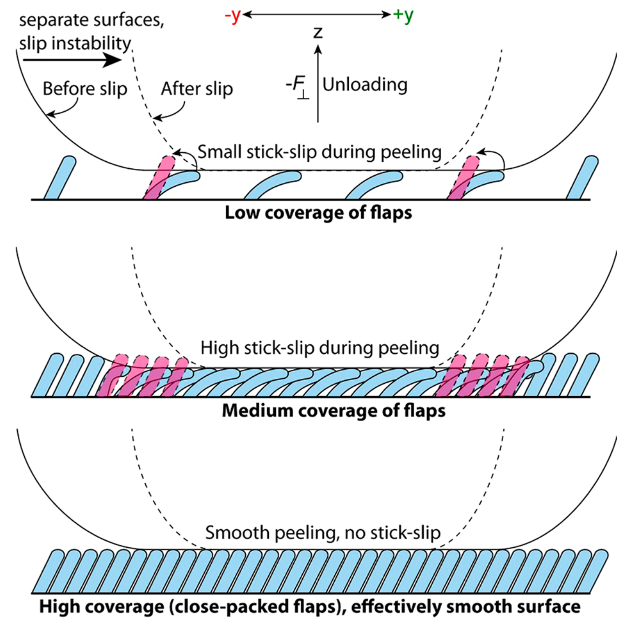

Figure 7. The magnitude of stick−slip instabilities observed in the load and friction forces (See Figures 6a and) during the peeling of the spherical glass disc from the patterned surface increases with increase in the flap density and would disappear eventually resulting in smooth peeling. This observation can be attributed to the number of flaps undergoing detachment during slip instability in the system. The flaps undergoing slip during instability are shown in red.

shearing along the +y direction could be large energy dissipation at the PDMS−silica interface close to the crack tip caused by the viscoelastic behavior of the polymer.[44] The latter possibility is more probable since the separation of the surfaces causes local elastic instabilities close to the crack tip, and this is evident from the graph of $F_{\perp}$ vs t (Figure 6).

Thus, if a material disperses its elastic energy in the form of waves into the bulk during separation of the surfaces with prior sliding along a specific direction, high adhesion energy will be attained maintaining good bonding to the surface. Alternatively, if prior sliding in a different direction causes the crack tip to move slowly during unloading of the two surfaces, the elastic energy would help assist the detachment process, thus mimicking the gecko adhesive system.

Shearing induced a significant change in the K_{eff} for the arrays of the microflaps (for both the 1X (low density) and the 3.5X (high density)) compared to pure loading and unloading with no prior shearing against the silica surface. This large value for the observed K_{eff} is due to the high elastic strain energy stored in the severely deformed flaps as a result of shearing of the surfaces. The stiffness was found to be similar for unloading of the flaps with prior shearing along the +y (along the direction of the tilt) or −y directions (against the direction of the tilt) for the 1X (Figures 4) and the 3.5X (Figures 5) respectively, meaning that the elastic energies for the deformation of the flaps along the +y and −y directions are similar. The observed effective degrees of stiffness were similar along both the directions (±y) since the flaps underwent severe deformations during the sliding of the surfaces and the inelastic property of the PDMS material determines the stiffness of the system. The tilt is important in determining the bending modulus only for small deflection of the flaps.[45]

This implies that the disparity in the adhesive strengths due to shearing of the surfaces along the two different directions is due to different real areas of contact between the PDMS flaps and silica surface during the sliding cycles and/or elastic instabilities, as explained above, and not due to the difference in the bending energies of the flaps as previously hypothesized.[11]

■ CONCLUSIONS

Our experimental results demonstrate that the Johnson–Kendall–Roberts (JKR) theory, using an effective surface energy and stiffness at the macro scale, quantitatively describes the contact mechanics of the microflaps ensemble against a smooth silica surface. The effective stiffness and the surface energy depend on the ratio of real to apparent contact areas, which can be measured in the SFA experiments. Inserting these values in the JKR theory yielded normal load vs area curves close to those measured, thereby validating this model. We also find an increasing adhesion and stick–slip of the surfaces during detachment, which we explain qualitatively in terms of the density of flaps, considering it to increase from 0% (no flaps, smooth surface) to 100% (close-packed flaps, effectively smooth surface). Our results and interpretations should be applicable to other rough and patterned surfaces and could serve as a model for designing and fabrication of gecko mimetic surfaces.

■ ASSOCIATED CONTENT

Ⓢ Supporting Information

The stress vs strain curve for bulk PDMS and the stick–slip peeling instabilities in the low density (1X) tilted PDMS flaps. This material is available free of charge via the Internet at http://pubs.acs.org.

■ AUTHOR INFORMATION

Corresponding Author

*E-mail:turner@engineering.ucsb.edu (K.L.T.); jacob@engineering.ucsb.edu (J.N.I.).

Notes

The authors declare no competing financial interest.

■ ACKNOWLEDGMENTS

The fabrication of micro flaps and rough surfaces was sponsored by the Institute for Collaborative Biotechnologies Grant No. DAAD19-03-D-0004 from the U.S. Army Research Office. The development of the 3D SFA and measurements of frictional adhesion were supported by the U.S. Department of Energy, Office of Basic Energy Sciences, Division of Materials Sciences and Engineering under Award No. DE-FG02-87ER-45331. The fabrication of PDMS flaps was done in the UCSB nanofabrication facility, part of the NSF-funded National Nanotechnology Infrastructure Network (NNIN). The SEM images were taken at the MRL Shared Experimental Facilities, which is supported by the MRSEC Program of the National Science Foundation under Award NSF DMR 1121053; a member of the NSF-funded Materials Research Facilities Network.

■ REFERENCES

(1) Autumn, K.; Hsieh, S. T.; Dudek, D. M.; Chen, J.; Chitaphan, C.; Full, R. J. Dynamics of geckos running vertically. *J. Exp. Biol.* **2006**, *209*, 260–272.

(2) Ruibal, R.; Ernst, V. Structure of digital setae of lizards. *J. Morphol.* **1965**, *117*, 271–293.

(3) Tian, Y.; Pesika, N.; Zeng, H. B.; Rosenberg, K.; Zhao, B. X.; McGuiggan, P.; Autumn, K.; Israelachvili, J. Adhesion and friction in gecko toe attachment and detachment. *Proc. Natl. Acad. Sci. U. S. A.* **2006**, *103*, 19320–19325.

(4) Pesika, N. S.; Tian, Y.; Zhao, B.; Rosenberg, K.; McGuiggan, P.; Autumn, K.; Israelachvili, J. N. Peel zone model of tape peeling based on the gecko adhesive system. *J. Adhes.* **2007**, *83*, 383–401.

(5) Pesika, N. S.; Gravish, N.; Wilkinson, M.; Zhao, B. X.; Zeng, H. B.; Tian, Y.; Israelachvili, J.; Autumn, K. The crowding model as a tool to understand and fabricate gecko-inspired dry adhesives. *J. Adhes.* **2009**, *85*, 512–525.

(6) Autumn, K.; Sitti, M.; Liang, Y. C. A.; Peattie, A. M.; Hansen, W. R.; Sponberg, S.; Kenny, T. W.; Fearing, R.; Israelachvili, J. N.; Full, R. J. Evidence for van der Waals adhesion in gecko setae. *Proc. Natl. Acad. Sci. U. S. A.* **2002**, *99*, 12252–12256.

(7) Hansen, W. R.; Autumn, K. Evidence for self-cleaning in gecko setae. *Proc. Natl. Acad. Sci. U. S. A.* **2005**, *102*, 385–389.

(8) Autumn, K.; Peattie, A. M. Mechanisms of adhesion in geckos. *Integr. Comp. Biol.* **2002**, *42*, 1081–1090.

(9) Zhou, M.; Pesika, N.; Zeng, H. B.; Wan, J.; Zhang, X. J.; Meng, Y. G.; Wen, S. Z.; Tian, Y. Design of gecko-inspired fibrillar surfaces with strong attachment and easy-removal properties: A numerical analysis of peel-zone. *J. R. Soc. Interface* **2012**, *9*, 2424–2436.

(10) Yu, J.; Chary, S.; Das, S.; Tamelier, J.; Turner, K. L.; Israelachvili, J. N. Friction and adhesion of gecko-inspired PDMS flaps on rough surfaces. *Langmuir* **2012**, *28*, 11527–11534.

(11) Yu, J.; Chary, S.; Das, S.; Tamelier, J.; Pesika, N. S.; Turner, K. L.; Israelachvili, J. N. Gecko-inspired dry adhesive for robotic applications. *Adv. Funct. Mater.* **2011**, *21*, 3010–3018.

(12) Jin, K.; Tian, Y.; Erickson, J. S.; Puthoff, J.; Autumn, K.; Pesika, N. S. Design and fabrication of gecko-inspired adhesives. *Langmuir* **2012**, *28*, 5737–5742.

(13) Autumn, K.; Dittmore, A.; Santos, D.; Spenko, M.; Cutkosky, M. Frictional adhesion: A new angle on gecko attachment. *J. Exp. Biol.* **2006**, *209*, 3569–3579.

(14) Huber, G.; Mantz, H.; Spolenak, R.; Mecke, K.; Jacobs, K.; Gorb, S. N.; Arzt, E. Evidence for capillarity contributions to gecko adhesion from single spatula nanomechanical measurements. *Proc. Natl. Acad. Sci. U. S. A.* **2005**, *102*, 16293–16296.

(15) Kim, T. W.; Bhushan, B. The adhesion model considering capillarity for gecko attachment system. *J. R. Soc. Interface* **2008**, *5*, 319–327.

(16) Niewiarowski, P. H.; Lopez, S.; Ge, L.; Hagan, E.; Dhinojwala, A. Sticky gecko feet: The role of temperature and humidity. *PLoS One* **2008**, *3*.

(17) Prowse, M. S.; Wilkinson, M.; Puthoff, J. B.; Mayer, G.; Autumn, K. Effects of humidity on the mechanical properties of gecko setae. *Acta Biomater.* **2011**, *7*, 733–738.

(18) Sun, W. X.; Neuzil, P.; Kustandi, T. S.; Oh, S.; Samper, V. D. The nature of the gecko lizard adhesive force. *Biophys. J.* **2005**, *89*, L14–L17.

(19) Autumn, K.; Liang, Y. A.; Hsieh, S. T.; Zesch, W.; Chan, W. P.; Kenny, T. W.; Fearing, R.; Full, R. J. Adhesive force of a single gecko foot-hair. *Nature* **2000**, *405*, 681–685.

(20) Zhao, B. X.; Pesika, N.; Rosenberg, K.; Tian, Y.; Zeng, H. B.; McGuiggan, P.; Autumn, K.; Israelachvili, J. Adhesion and friction force coupling of gecko setal arrays: Implications for structured adhesive surfaces. *Langmuir* **2008**, *24*, 1517–1524.

(21) Campolo, D.; Jones, S.; Fearing, R. S. In *Fabrication of Gecko Foot-Hair Like Nano Structures and Adhesion to Random Rough Surfaces; Nanotechnology, 2003*; Third IEEE Conference on, 12–14 Aug. 2003; IEEE-NANO: 2003, pp 856–859; Vol. 2.

(22) Murphy, M. P.; Kim, S.; Sitti, M. Enhanced adhesion by gecko-inspired hierarchical fibrillar adhesives. *ACS Appl. Mater. Interfaces* **2009**, *1*, 849–855.

(23) Kamperman, M.; Kroner, E.; del Campo, A.; McMeeking, R. M.; Arzt, E. Functional adhesive surfaces with "gecko" effect: The concept of contact splitting. *Adv. Eng. Mater.* **2010**, *12*, 335−348.

(24) Canas, N.; Kamperman, M.; Volker, B.; Kroner, E.; McMeeking, R. M.; Arzt, E. Effect of nano- and micro-roughness on adhesion of bioinspired micropatterned surfaces. *Acta Biomater.* **2012**, *8*, 282−288.

(25) Lee, H.; Lee, B. P.; Messersmith, P. B. A reversible wet/dry adhesive inspired by mussels and geckos. *Nature* **2007**, *448*, 338−341.

(26) Murphy, M. P.; Aksak, B.; Sitti, M. Gecko-inspired directional and controllable adhesion. *Small* **2009**, *5*, 170−175.

(27) He, L. W.; Yan, S. P.; Li, B. Q.; Chu, J. R. Directional adhesion behavior of a single elastic fiber. *J. Appl. Phys.* **2012**, *112*, 013516.

(28) Qu, L. T.; Dai, L. M.; Stone, M.; Xia, Z. H.; Wang, Z. L. Carbon nanotube arrays with strong shear binding-on and easy normal lifting-off. *Science* **2008**, *322*, 238−242.

(29) Yurdumakan, B.; Raravikar, N. R.; Ajayan, P. M.; Dhinojwala, A. Synthetic gecko foot-hairs from multiwalled carbon nanotubes. *Chem. Commun. (Cambridge, U. K.)* **2005**, 3799−3801.

(30) Jeong, H. E.; Kwak, M. K.; Suh, K. Y. Stretchable, adhesion-tunable dry adhesive by surface wrinkling. *Langmuir* **2010**, *26*, 2223−2226.

(31) Geim, A. K.; Dubonos, S. V.; Grigorieva, I. V.; Novoselov, K. S.; Zhukov, A. A.; Shapoval, S. Y. Microfabricated adhesive mimicking gecko foot-hair. *Nat. Mater.* **2003**, *2*, 461−463.

(32) Persano, L.; Dagdeviren, C.; Su, Y. W.; Zhang, Y. H.; Girardo, S.; Pisignano, D.; Huang, Y. G.; Rogers, J. A. High performance piezoelectric devices based on aligned arrays of nanofibers of poly(vinylidenefluoride-*co*-trifluoroethylene). *Nat. Commun.* **2013**, 4.

(33) Silberzan, P.; Perutz, S.; Kramer, E. J.; Chaudhury, M. K. Study of the self-adhesion hysteresis of a siloxane elastomer using the JKR method. *Langmuir* **1994**, *10*, 2466−2470.

(34) Israelachvili, J.; Min, Y.; Akbulut, M.; Alig, A.; Carver, G.; Greene, W.; Kristiansen, K.; Meyer, E.; Pesika, N.; Rosenberg, K.; Zeng, H. Recent advances in the surface forces apparatus (SFA) technique. *Rep. Prog. Phys.* **2010**, *73*, 036601.

(35) Bhushan, B. *Introduction to Tribology*; John Wiley & Sons: New York, 2002.

(36) Johnson, K. L.; Kendall, K.; Roberts, A. D. Surface energy and contact of elastic solids. *Proc. R. Soc. London A* **1971**, *324*, 301−313.

(37) Israelachvili, J. N. *Intermolecular and Surface Forces*, 3rd ed.; Academic Press: Burlington, MA, 2011.

(38) Yang, C.; Persson, B. N. J.; Israelachvili, J.; Rosenberg, K. Contact mechanics with adhesion: Interfacial separation and contact area. *Europhys. Lett.* **2008**, *84*, 46004.

(39) Benz, M.; Rosenberg, K. J.; Kramer, E. J.; Israelachvili, J. N. The deformation and adhesion of randomly rough and patterned surfaces. *J. Phys. Chem. B* **2006**, *110*, 11884−11893.

(40) Fuller, K. N. G.; Tabor, D. Effect of surface-roughness on adhesion of elastic solids. *Proc. R. Soc. London, A* **1975**, *345*, 327−342.

(41) Maugis, D. Adhesion of spheres—The JKR-DMT transition using a Dugdale model. *J. Colloid Interface Sci.* **1992**, *150*, 243−269.

(42) Carpick, R. W.; Ogletree, D. F.; Salmeron, M. A general equation for fitting contact area and friction vs load measurements. *J. Colloid Interface Sci.* **1999**, *211*, 395−400.

(43) Schallamach, A. A theory of dynamic rubber friction. *Wear* **1963**, *6*, 375−382.

(44) Mulakaluri, N.; Persson, B. N. J. Adhesion between elastic solids with randomly rough surfaces: Comparison of analytical theory with molecular-dynamics simulations. *Europhys. Lett.* **2011**, *96*, 66003.

(45) Autumn, K.; Majidi, C.; Groff, R. E.; Dittmore, A.; Fearing, R. Effective elastic modulus of isolated gecko setal arrays. *J. Exp. Biol.* **2006**, *209*, 3558−3568.